Applied Mathematics and Computation 215 (2010) 3655–3664

Contents lists available at ScienceDirect

Applied Mathematics and Computation

journal homepage: www.elsevier.com/locate/amc

A hybrid convex variational model for image restoration

V.B. Surya Prasath, Arindama Singh *

Department of Mathematics, Indian Institute of Technology Madras, Chennai 600036, India

ARTICLE INFO

Keywords:
Image restoration
Regularization
Nonlinear diffusion
Convex filters

ABSTRACT

We propose a new hybrid model for variational image restoration using an alternative diffusion switching non-quadratic function with a parameter. The parameter is chosen adaptively so as to minimize the smoothing near the edges and allow the diffusion to smooth away from the edges. This model belongs to a class of edge-preserving regularization methods proposed in the past, the ϕ-function formulation. This involves a minimizer to the associated energy functional. We study the existence and uniqueness of the energy functional of the model. Using real and synthetic images we show that the model is effective in image restoration.

1. Introduction

Image restoration is one of the early tasks in computer vision. It may be modeled by an equation of the form:

$$u_0 = Tu + n, \tag{1}$$

where u is the original image, u_0 is the noisy blurred image and n represents the additive white Gaussian noise with mean 0 and variance σ_n^2. We assume, in the continuous setting, that $T : L^2(\Omega) \to L^2(\Omega)$ is a blur operator (linear and bounded), usually a convolution. The linear equation (1) is generally ill-posed. To overcome this, regularization techniques are widely employed in restoring the images [1,2], see [3] for a review. The classical Tikhonov regularization [4] corresponds to minimizing the functional

$$E(f) = \int_\Omega |u_0 - Tu|^2 + \alpha \int_\Omega |\nabla f|^2, \tag{2}$$

where the regularization parameter α acts as a balancing factor between the fidelity term and the smoothing term. This quadratic case is usually considered a prime example of linear regularization methods in image restoration. If we assume the blur operator T is such that $T.1 \neq 0$ then the minimization of $E(u)$ in Eq. (2) admits a unique solution in the space $H^1(\Omega)$. The corresponding Euler–Lagrange equation is

$$T^* Tu - T^* u_0 - \alpha \Delta u = 0 \tag{3}$$

which is a uniformly elliptic PDE having strong smoothing properties. This gives rise to smearing of the edges in the restored image. To alleviate this the ϕ-function formulation was introduced by Aubert and Vese [5]. Instead of minimizing $E(.)$ in (2), they proposed the minimization of

$$E(u) = \int_\Omega |u_0 - Tu|^2 + \alpha \int_\Omega \phi(|\nabla u|), \tag{4}$$

* Corresponding author.
E-mail addresses: surya.iit@gmail.com (V.B. Surya Prasath), asingh@iitm.ac.in (A. Singh).

0096-3003/$ - see front matter
doi:10.1016/j.amc.2009.11.003

where $\alpha \geqslant 0$ is a weight parameter and $\phi : \mathbb{R} \to \mathbb{R}^+$ is an even, convex and nondecreasing function. The Euler–Lagrange equation for (4) in the gradient descent form is the diffusion equation given by

$$\frac{\partial u}{\partial t} = \alpha\, div\Big(\frac{\phi'(|\nabla u|)}{|\nabla u|}\nabla u\Big) - (T^*Tu - T^*u_0). \tag{5}$$

This diffusion equation belongs to a class of anisotropic nonlinear diffusion equations first proposed by Perona–Malik [6] in the special form

$$\frac{\partial u}{\partial t} = \alpha\, div(g(|\nabla u|)\nabla u) - (T^*Tu - T^*u_0), \tag{6}$$

where $g(.)$ is a decreasing function so chosen to reduce the diffusion near the edges. Notice that (6) is obtained from (5) by taking ϕ so that

$$\phi'(s) = g(s)s. \tag{7}$$

The regularization parameter α controls the *speed* of the diffusion. In the original ϕ-formulation, α is fixed either by heuristic methods or by classical parameter selection methods. In this paper we propose a new model which automatically selects the amount of smoothing by changing the parameter adaptively and by using a new function ϕ which satisfies the edge-preserving regularizing properties. This particular class of functions ϕ provides us a simple existence and uniqueness result for the minimizer of the corresponding energy functional $E(.)$.

The paper is organized as follows: Section 2 discusses the model. In Section 3 we give theoretical justification for using the model. Section 4 discusses and compares the other related methods proposed in the literature. Numerical simulations to show the robustness of the model are included in Section 5. Section 6 concludes the paper.

2. The model

We consider the spatially adaptive model of the ϕ-formulation (4)

$$E(u) = \int_\Omega |u_0 - Tu|^2 + \int_\Omega \alpha(x)\phi(|\nabla u|), \tag{8}$$

where α is a continuous function on Ω. Moreover to decrease the diffusion near edges, we take $\alpha \approx 0$ near the edges. For example one can choose (see [7])

$$\alpha(x) = \frac{1}{1 + |\nabla G_\sigma \star u_0(x)|}, \tag{9}$$

where $\star$ denotes the convolution. To avoid the false detections due to noise, we take convolution of the gradient of the given data g with Gaussian kernel $G_\sigma := C\sigma^{-1}\exp(-|x|^2/2\sigma)$. The choice of ϕ is such that when $|\nabla u|$ is less than the edge threshold M, isotropic smoothing is preferred, and when there are edges the power of smoothing is reduced by an amount of $|\nabla u|$ producing the anisotropic smoothing. Further, the function ϕ must be chosen so as to satisfy the following principle of image analysis:

the reconstructed image consists of homogeneous (flat) regions separated by sharp edges (discontinuities).

We take

$$\phi(s) = \begin{cases} as^2, & \text{for } s \leqslant M, \\ bs^2 + cs + d, & \text{for } s > M, \end{cases} \tag{10}$$

where $a, b, c, d > 0$ and $M > 0$ is the threshold specifying the relative edge strength. As in [5] we extend the function to be an even function, $\Phi(\nabla u) = \phi(|\nabla u|)$. The physical meaning of this ϕ can be explained by looking at the corresponding PDE (6) using the relation (7). In our case when $s \leqslant M,\ g(s) = \phi\prime(s)/s = 2a$ gives the heat equation (isotropic smoothing) and when $s > M$ we have $g(s) = 2b + c/s$ giving the total variation (TV) type flow [8]. At all other locations ϕ self-adjusts to use the appropriate combination of both isotropic smoothing and TV. Furthermore, the function (10) is both strictly convex and lower semi-continuous. This leads to a mathematically sound model.

Fig. 1 illustrates this for different b values with $a = 8$. The solid line represents the g corresponding to the parameter $b = 1$, dashed and dotted lines refer to $b = 0.5$ and $b = -1$, respectively. The edge threshold M determines the switching from high value $2a$ to low value $2b$ with transition rate $O(s^{-1})$. Detailed comments about the numerical implementation of the choices of ϕ-function parameters are discussed in Section 4.

We note that the transition is rather slow compared to the hard thresholding example of Chambolle and Lions [9], who took

$$\phi(s) = \begin{cases} s^2, & \text{for } s \leqslant M, \\ s, & \text{for } s > M. \end{cases} \tag{11}$$

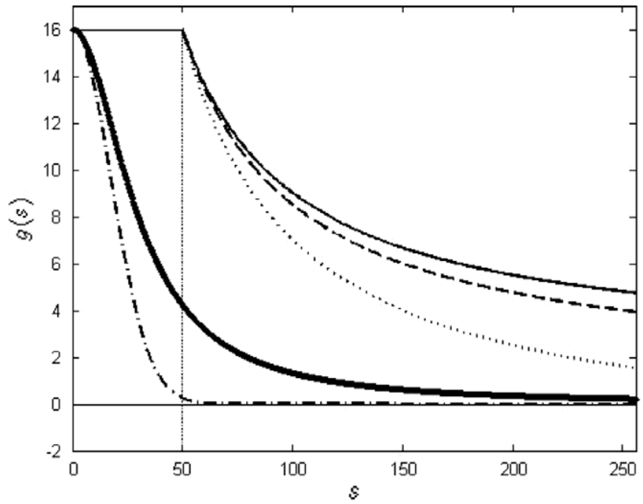

Fig. 1. Different $g(.)$ using (10) with $a = 8,\ M = 50$. Solid line corresponds to $b = 1$, dashed line corresponds to $b = 0.5$ and dotted line corresponds to $b = -1$. The other two functions are g_1 (dark line), g_2 (dash-dotted line) proposed by Perona–Malik in [6], they decay faster than the proposed functions here.

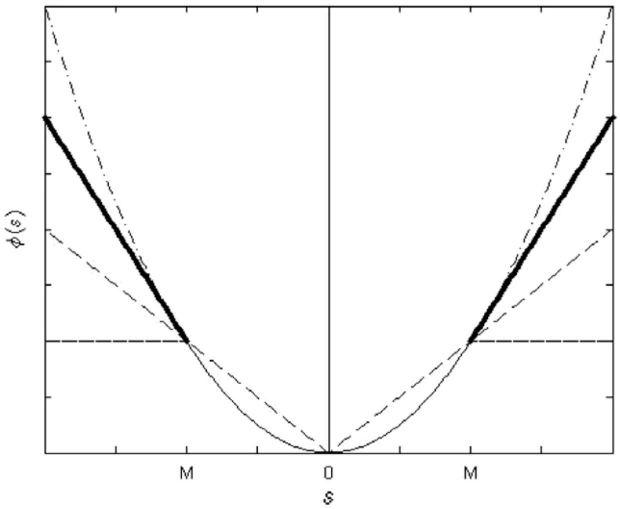

Fig. 2. Comparison of ϕ functions. The dark line represents the functions proposed in this paper, it is intermediate between global TV function $\phi(s) = s$ dashed line and $\phi(s) = s^2$ dash-dotted line. The thin line is $\phi(s) = \min\{as^2, C\}$.

Moreover, the model in [9] uses the notion of inf-convolution, in contrast to the simple existence theory of our model. This difference is due to the fact that in our model, when $s > M$ the decrease is not in the order of s but rather in $bs^2 + cs + d$. Ideally we want $b \ll a$, so that the effect of the quadratic term in the function is reduced when the edges are present. Fig. 2 illustrates this behavior with other global schemes namely, the quadratic $\phi(s) = s^2$, TV $\phi(s) = s$, and the model proposed in [10], $\phi(s) = \min\{as^2, C\},\ C > 0$ constant. The lines which lies in between the isotropic and TV model corresponds to (10). By changing the value of b and by the adaptive nature of α we get different anisotropic flows which are intermediate between these global models. Unlike the TV function $\phi(s) = s$ or $\phi(s) = \min\{as^2, C\}$, ϕ in (10) is differentiable at every point.

The choice of the regularization parameter α is motivated by the following considerations. The function α controls the speed of diffusion as is evident from

$$\frac{\partial u}{\partial t}(x,t) = div(\alpha(x) g(|\nabla u|)\nabla u) - (T^*Tu - Tu_0) \tag{12}$$

which is the Euler–Lagrange equation in the gradient descent form for the functional $E(.)$ in (8). The parameter $\alpha(x)$ adjusts itself according to the smoothed edge information at x so as to reduce the speed of diffusion near the edges. Also, one can use the updated version of the image in (9) instead of the given noisy image g. That is

$$\alpha(x) = \frac{1}{1 + |\nabla G_\sigma \star u(x)|} \tag{13}$$

can be used to update the edge information at x. In general one can choose regularizing parameter $\alpha(x)$ satisfying the α-condition put forth by [7]. The consistency of the model (Section 3) holds true for these choices of α's as in (9) and (13) as long as we have

$$\sup_{x\in\Omega} |\alpha(x)| < \infty.$$

This condition is automatically satisfied for continuous functions α on a compact set Ω. For digital images Ω is usually a rectangle or a square, hence the continuity of the function α is sufficient.

3. Consistency of the model

In the sequel we use the following result about an operator equation involving the framework of monotone operators (see [11, Section 25]). Here $\|\cdot\|_H$ is the norm on the Hilbert space H. $\|\cdot\|_{H^*}$ is the corresponding norm on the dual space H^*. $\langle , \rangle$ is the bilinear pairing between H^* and H.

Theorem 1. *Let H be a real separable Hilbert space, and let the functional $E : H \to \mathbb{R}$ be weakly coercive, i.e.,*

$$E(u) \to \infty as \|u\|_H \to \infty.$$

Suppose that E is Gâteux differentiable and the derivative is Lipschitz continuous and strongly monotone, i.e., there are numbers $K > 0$ and $c > 0$ such that, for all $h, l \in H$,

$$\|E'(h) - E'(l)\|_{H^*} \leqslant K\|h - l\|_H$$

and

$$\langle E'(h) - E'(l), h - l\rangle \geqslant c\|h - l\|_H^2.$$

Then the problem $\min_f E(f)$ has a unique solution $f \in H$.

We use Theorem 1 to find the minimum of the functional $E(.)$, or equivalently, the critical point of $E\prime(.)$ for the functional E introduced in Eq. (8). As noted in Section 1, the derivative gives rise to the Perona–Malik type anisotropic equation when written in the gradient descent form (12). We prove the following:

Theorem 2. *Let $\Omega \subset \mathbb{R}^N$ be a closed and bounded domain. Suppose $u_0 : \Omega \to \mathbb{R}$ is the given image and $\alpha : \Omega \to \mathbb{R}$ is a continuous function. Let the regularization function in (10) with $a, b > 0$, $c = 2M(a - b)$ and $d = -M^2(a - b)$. Then the functional $E(u)$ defined in (8) has a unique minimizer $u \in H^1(\Omega)$.*

Proof. We first show that the functional $E(.)$ is well defined and continuous: From the definition of ϕ in (10), we have

$$|\Phi(s)| \leqslant a|s|^2, \quad \text{for all } s \in \mathbb{R}^N. \tag{14}$$

Let $M_\alpha = \sup_{x\in\Omega}|\alpha(x)|$ and $\Psi(x, u, \nabla u) = |(u_0 - Tu)(x)|^2 + \alpha(x)\Phi(\nabla u)$ be the integrand of E in (8). Then

$$|\Psi| \leqslant 2u_0^2 + C(u^2 + |\nabla u|^2)$$

with $C = \max\{2, aM_\alpha\}$. If a sequence $u_n \to u$ in H^1 then $\nabla u_n \to \nabla u$ and $\Psi(x, u_n, \nabla u_n) \to \Psi(x, u, \nabla u)$. So E is continuous.

We check that our functional $E(.)$ satisfies the assumptions of Theorem 1. From (10), we see that E is weakly coercive as $\Phi(s)$ is strictly convex

$$(\Phi'(s) - \Phi'(t)) \cdot (s - t) \geqslant 2b|s - t|^2, \quad \text{for all } s, t \in \mathbb{R}^N.$$

Considering the first variation of E at $h \in H^1$ given by

$$\langle E'(u), h\rangle = \int_\Omega \{2(u_0 - Tu)h + \alpha(x)\Phi'(\nabla u) \cdot \nabla h\} dx \tag{15}$$

we see that E' is a C^1-function. For, if a sequence $u_n \to u$ in H^1, then $\nabla u_n \to \nabla u$. From (10), we obtain

$$|\Phi'(s) - \Phi'(t)| \leqslant 6a|s - t|, \quad \text{for all } s, t \in \mathbb{R}^N. \tag{16}$$

Then using (15) and (16), we obtain

$$\begin{aligned} |\langle E'(u_n) - E'(u), h\rangle| &= \int_\Omega |2(Tu_n - Tu)h| dx + \int_\Omega |(\alpha(x)\Phi'(\nabla u_n) - \alpha(x)\Phi'(\nabla u)) \cdot \nabla h| dx \\ &\leqslant 2\|T\|\|u_n - u\|_2\|h\|_2 + 6aM_\alpha\|\nabla u_n - \nabla u\|_2\|\nabla h\|_2, \end{aligned}$$

where $\|\cdot\|_2$ denotes the $L^2(\Omega)$ norm. Since the above inequality holds for every $h \in H^1$ we have $E'(u_n) \to E'(u)$. Also E' is Lipschitz continuous in H^1 as,

$$|\langle E'(h) - E'(l), k\rangle| \leqslant 2\|T\|\|h-l\|_2\|k\|_2 + 6aM_\alpha\|\nabla h - \nabla l\|_2\|\nabla k\|_2 \leqslant \max\{2\|T\|, 6aM_\alpha\}\|h-l\|_{H^1}\|k\|_{H^1}.$$

E' is strongly monotone, as

$$\langle E'(h) - E'(l), h-l\rangle = \int_\Omega \{2(h-l)^2 + (\alpha(x)\Phi'(\nabla h) - \alpha(x)\Phi'(\nabla l))\cdot(\nabla h - \nabla l)\}dx$$
$$\geqslant \min\{2\|T\|, 2bM_\alpha\}\int_\Omega\{(h-l)^2 + |\nabla h - \nabla l|^2\}dx = \min\{2\|T\|, 2bM_\alpha\}\|h-l\|_{H^1}.$$

Thus our functional $E(.)$ given in (8) satisfies the assumptions of Theorem 1. Hence $E(.)$ has a unique minimizer. □

We have proved the existence of the minimizer in $H^1(\Omega)$, a similar result in the space of functions of bounded variation $BV(\Omega)$ can be obtained, see [3].

Theorem 3. *Let $\Omega \subset \mathbb{R}^N$ be a closed and bounded domain. Suppose $u_0 \in BV(\Omega) \cap L^2(\Omega)$ is the given image and $\alpha : \Omega \to \mathbb{R}$ is a continuous function. Then the functional $E(u)$ defined in (8) has a unique minimizer $u \in BV(\Omega) \cap L^2(\Omega)$.*

Proof. The functional $E(u)$ is strictly convex and coercive as shown in Theorem 2. The functional $E(u)$ is lower semi-continuous in $BV(\Omega) \cap L^2(\Omega)$. Thus, by Theorem 3.2.2 in [3], the corresponding minimization problem (3) has a unique solution in $BV(\Omega) \cap L^2(\Omega)$. □

4. Discussion

The function ϕ given in (10) is a combination of two smooth functions; it alternates between the quadratic smoothing and a more general quadratic behavior. Fig. 3 shows the second part of the function ϕ in (10) for different values of b with $M = 50$. The solid line represents the ϕ corresponding to the parameter $b = 1$, dashed and dash-dotted lines refer to $b = 0.5$ and $b = -1$, respectively. Since ϕ is a C^1-function, $c = 2M(a-b)$ and $d = -M^2(a-b)$, we need to choose only the constants a and b. As noted before to reap the benefit of the anisotropic diffusion when there are no edges, and the total variation when the edges are present, we choose $b \ll a$.

The first term in (10) implies the smoothing of the image. The parameter a can be chosen so as to maximize the isotropic smoothing in homogenous regions. In this case, the PDE is (by (7)):

$$\frac{\partial u}{\partial t}(x,t) = 2a\,div(\alpha(x)\nabla u) - (T^*Tu - T^*u_0), \tag{17}$$

where α is near one. The second term takes over when the edges are present. In this case, the PDE is:

$$\frac{\partial u}{\partial t}(x,t) = 2b\,div(\alpha(x)\nabla u) + c\,div\left(\alpha(x)\frac{\nabla u}{|\nabla u|}\right) - (T^*Tu - T^*u_0). \tag{18}$$

Here it is a combination of isotropic and total variation flow. Thus $b \ll a$ can be chosen so as to reduce the effect of the first term on the right hand side. Also, we observe that $b < 0$ adds a reverse diffusion flow term in the PDE (18). Inverse diffusion equation is used in image deblurring. Though it is ill-posed, choosing $b = -1$ in the experiments yields good restoration of images.

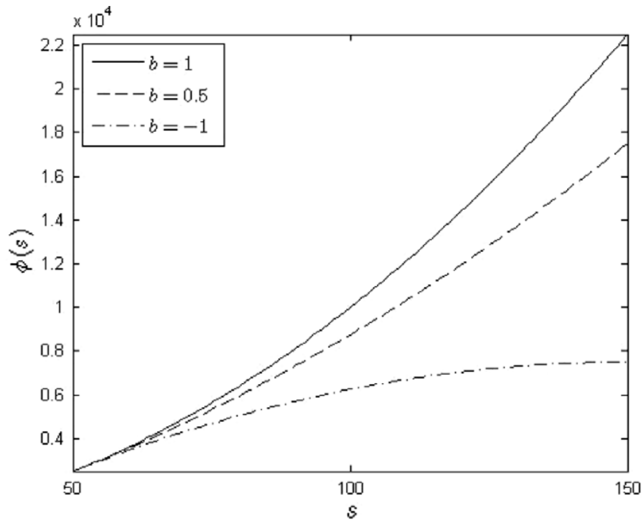

Fig. 3. The proposed function ϕ (10) for different b's. The solid line represents the ϕ corresponding to the parameter $b = 1$, dashed line $b = 0.5$ and dash-dotted lines refer to $b = -1$ case.

In all our experiments we choose $b < 0$ in such a way that g stays positive; hence inverse diffusion is controlled. This can be achieved by choosing the value of a accordingly. In this case, our existence theorem does not say anything. If $b < 0$ then the corresponding ϕ is concave in the region $s > M$ and its maximum value is attained at $s = -c/2b$. The corresponding diffusion function $g(s)$ becomes negative when $s > -c/2b$. By choosing a large value for a we can make $g(s)$ decrease faster than the other g's corresponding to $b > 0$ and still maintain the diffusion positive. This can be compared with the diffusion function $g_1(s) = (1 + (s/K)^2)^{-1}$ originally proposed by Perona–Malik [6] where K plays the role of edge threshold M. They have also proposed the function $g_2(s) = \exp(-(s/K)^2)$ which decays faster than the previous function, see Fig. 1. In contrast to the model proposed here their model has been proved to be ill-posed, see [12].

This negative b case is also similar to the concave balanced forward–backward (BFB) filters proposed in [13]. BFB filter diffusivity $g_3(s) = s^{-2}$ with the corresponding $\phi(s) = log(s)$ decreases faster than the diffusion functions derived from (10) (see Section 2). This tends to sharpen the image in a global manner rather than the method proposed here. The isotropic case corresponds to PDE (17) acts as a forward diffusion with strength $2a\alpha(x)$ in the homogenous regions. This implies Gaussian smoothing which is effective in removing the noise. On the other hand the hybrid total variation case corresponds to PDE (18) helps to retain the sharp edges. Also the spatially adaptive nature of the regularization parameter α allows the model to have a much lower dependence on the edge threshold M.

When $b = 0$, the function ϕ in (10) is

$$\phi(s) = \begin{cases} as^2 & \text{for } s \leqslant M, \\ 2Mas - M^2a & \text{for } s > M \end{cases}$$

which is the same as the Chambolle and Lions, see Eq. (11). In this case, since the function ϕ is not strictly convex, our existence theorem in Section 3 guarantees only the existence of a minimizer but not its uniqueness. Other related filters include edge-flat-grey (EFG) filters studied by Ito and Kunisch in [1], which includes a separate part in the regularization function to handle grey scales. Keeling [2] studied and compared such convex filters from medical imaging point of view, see also [14] for an application of them in diffusion tensor imaging.

5. Numerical examples

We apply the above PDEs (17) and (18) to real and synthetic images in the denoising case. Our initial data is $u(x,0) = u_0(x)$, and the natural Neumann boundary conditions are used. To avoid the dependency on the edge threshold, a histogram of the absolute values of the gradient throughout the image was computed, and M was set equal to the 90% value of its integral at every iteration. Division by zero is avoided in the second diffusion term of (18), adaptive TV term, by approximating $div(\alpha(x)\nabla u|\nabla u|^{-1})$ with $div(\alpha(x)\nabla f(|\nabla u|^2 + \epsilon^2)^{-1/2})$ for small ϵ. We approximated the PDEs using a explicit Euler scheme with central differences. Experimentally similar results were obtained using the minmod approximation [8] and we believe other difference schemes should work as well.

Fig. 4 shows the results for *Lena* image corrupted with an additive Gaussian noise of $\sigma_n = 20$. As indicated the experiments depend on the parameters a which determines the amount of forward smoothing and b which controls the isotropic smoothing term in the second PDE, Eq. (18). Fig. 4a shows the original image for comparison, and noisy image is given in Fig. 4b. The reconstructions with $b = 1$ (Fig. 4c) and $b = -1$ (Fig. 4d) with $a = 8$ in our function (10) are shown for comparison. We observe that reconstruction corresponding to b negative produces sharp results but with patchy effects (creation of stippled noise pattern) in homogeneous regions when the noise level is high. This is due to the fact that the hybrid TV term dominates the flow in (18) when b is negative.

In Fig. 5 we compare the Gaussian smoothing (isotropic) $g(s) = s^2$, TV $g(s) = s$ and Perona–Malik diffusion function $g_1(s) = (1 + (s/K)^2)^{-1}$ with our hybrid model on a synthetic *Shapes* image. The isotropic diffusion (Fig. 5c) removes the noise and reconstructs smooth regions but the edges are severely blurred. Perona–Malik diffusion (Fig. 5d) reconstructs the image better than the isotropic smoothing but over smooths the mid-tone grey valued left side square and big circle. The pure TV model (Fig. 5e) reconstructs the edges but the staircasing effect is clearly visible. By combining the two diffusions, namely the Gaussian smoothing and TV, the proposed method (Fig. 5f) overcomes these shortcomings and recovers the image almost perfectly.

Fig. 6 shows a profile line taken horizontally at the top half (pixel position 80) of the *Shapes* image in Fig. 5. Original signal is represented by the dotted line, the noisy signal by dots. The restored signals by Perona–Malik filter [6], TV filter [8] exhibit staircasing artifacts. Our scheme results in near perfect recovery of the signal without any staircasing effect and coincides with the original signal in this case.

Fig. 7 shows *Barbara* image restored with $a = 8$ and $b = 1$. Fig. 8 shows the closeup of Barbara image, which indicates that textures are also recovered well by our method. A PSNR analysis conducted on the standard test images (taken from USC-SIPI Image database) are listed in Tables 1 and 2. The peak signal-to-noise ratio (PSNR) is most commonly used as a measure of quality of reconstruction. PSNR for a grey scale image is defined as:

$$\mathrm{PSNR} = 10\log 10\left(\frac{255^2}{\mathrm{MSE}}\right). \tag{19}$$

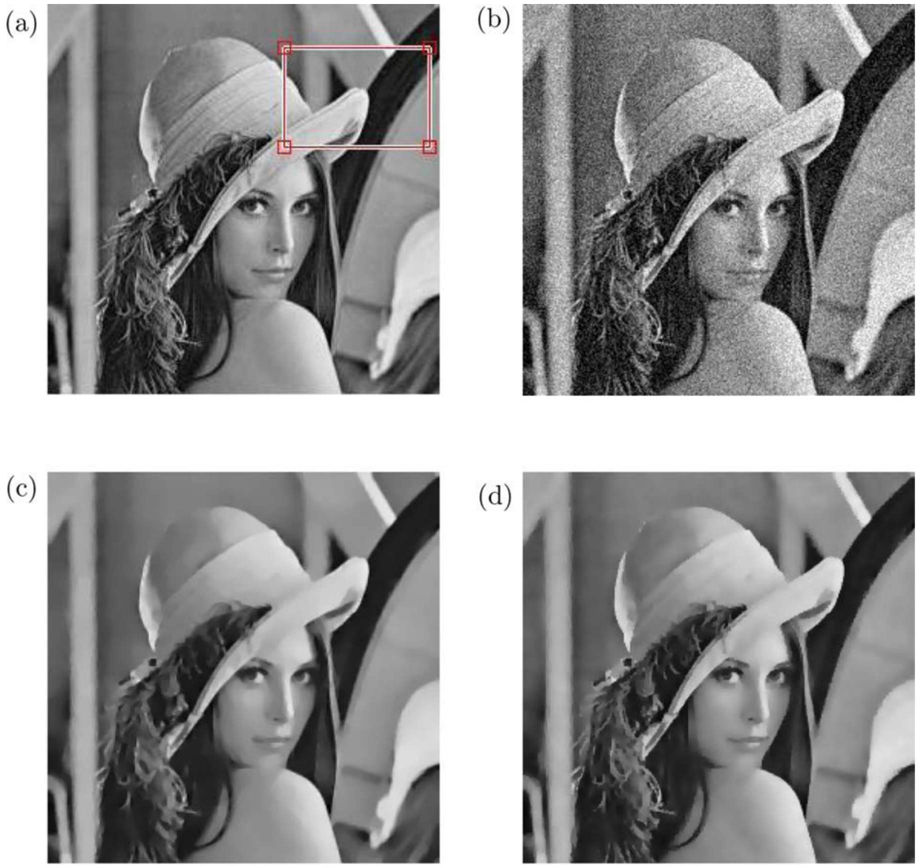

Fig. 4. Restoration of *Lena* image by the proposed scheme: (a) original image; (b) noisy with $\sigma_n = 20$; (c) restored with $b = 1$ and (d) restored with $b = -1$.

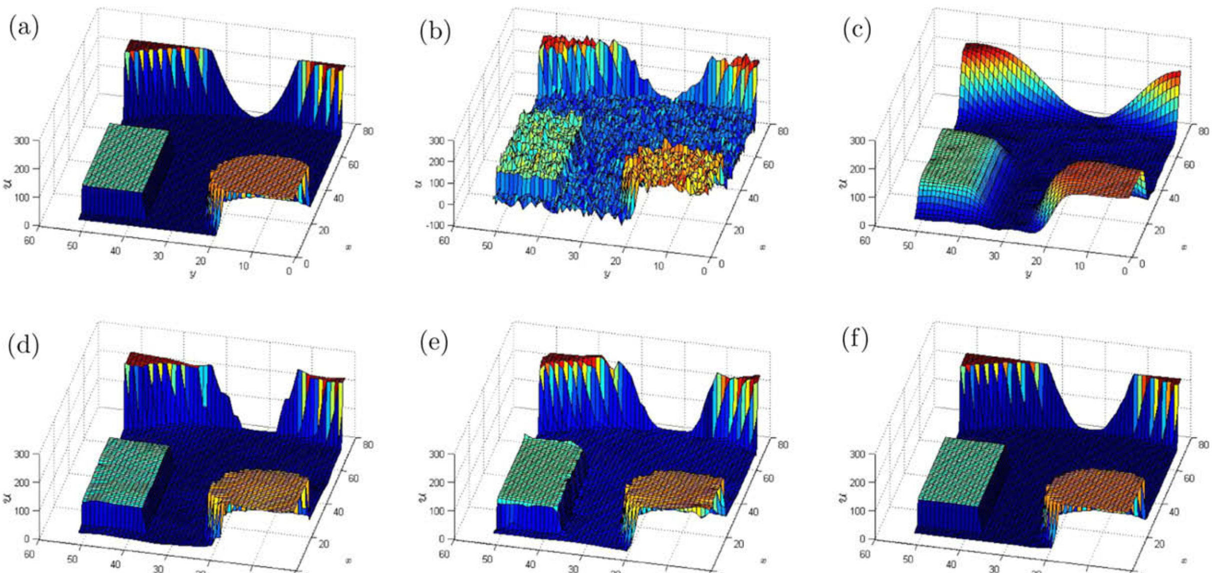

Fig. 5. Restoration of the *Shapes* image shown in surface form to highlight the staircasing artifacts and smoothing effects: (a) original; (b) noisy with $\sigma_n = 20$; (c) restored using isotropic diffusion; (d) Perona–Malik with g_1 diffusion function; (e) pure TV model and (f) our method.

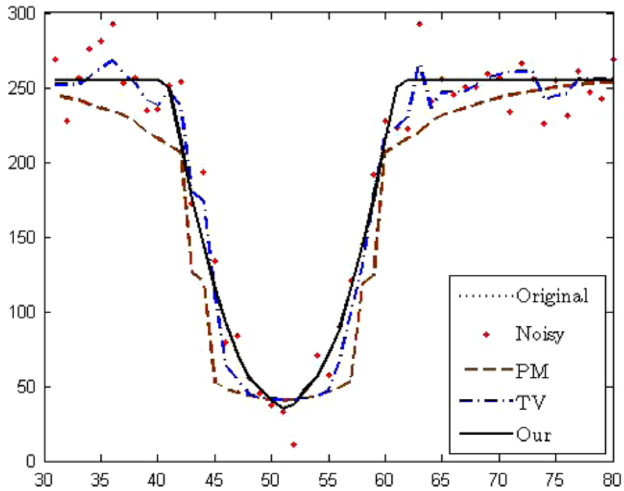

Fig. 6. Restoration of the *Shapes* 1D signal taken from Fig. 5a. PM and TV filters create staircasing artifacts in gradient scale regions whereas our scheme almost coincides with the original signal.

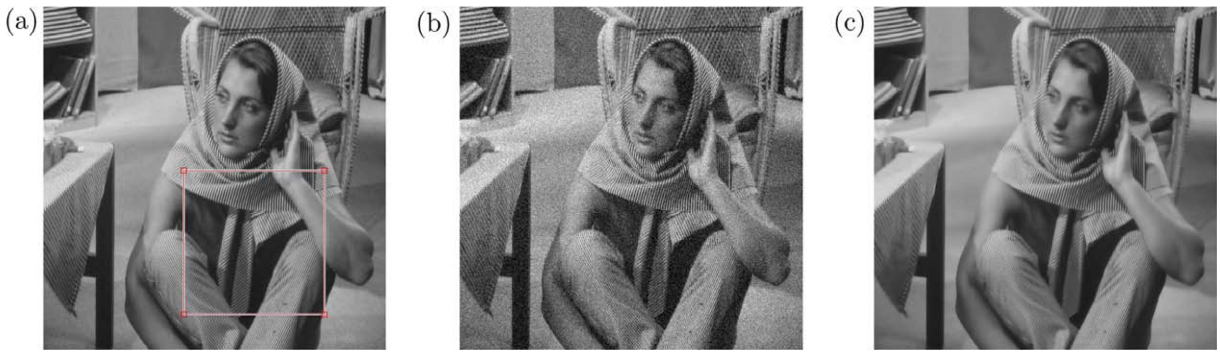

Fig. 7. Restoration of *Barbara* image: (a) original; (b) noisy image with $\sigma = 20$ and (c) restored by our scheme.

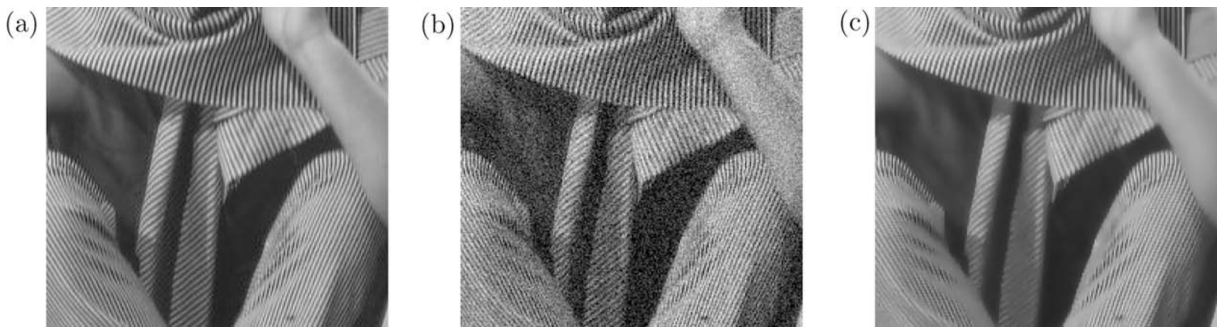

Fig. 8. Closeup of *Barbara* image from Fig. 7: (a) original; (b) noisy and (c) restored version.

Here MSE is the mean square error for two $m \times n$ monochrome images I and J, where one of the images is considered a noisy approximation of the other, is defined as:

$$\mathrm{MSE}(I,J) = \frac{\sum_{i,j}(I(i,j) - J(i,j))^2}{mn}.$$

Table 1 shows the PSNR analysis of the model with $a = 8,\ b = 1$ in (10). The column labelled 'noisy' at each noise level σ_n represents the PSNR value of the corrupted image when compared with the original image, and 'result' gives the PSNR of the

Table 1
PSNR (dB) results of the proposed model with $a = 8,\ b = 1$ for various noise levels. At each noise level 'noisy' column represents the PSNR of the noisy image and 'result' the resultant image by our scheme.

Noise images	$\sigma_n = 5$		$\sigma_n = 10$		$\sigma_n = 15$		$\sigma_n = 20$	
	Noisy	Result	Noisy	Result	Noisy	Result	Noisy	Result
Lena	37.18	38.39	32.04	34.77	30.19	33.19	29.32	32.20
Cameraman	37.22	38.65	32.22	34.53	30.42	33.27	29.53	32.18
Barbara	37.17	38.18	32.02	34.04	30.15	32.63	29.29	31.81
House	37.20	38.85	32.04	34.57	30.13	32.73	29.25	32.13
Baboon	37.15	37.62	32.01	33.04	30.06	31.65	29.33	31.01
Shapes	39.15	40.59	34.04	37.29	32.12	35.17	31.26	34.02
Peppers	37.18	38.43	32.13	34.09	30.20	32.89	29.35	32.31
Montage	37.19	39.49	32.08	35.09	30.22	33.92	29.38	33.14
Man	37.10	38.18	31.98	34.49	30.17	33.10	29.29	32.26
Boats	37.20	38.21	32.08	33.65	30.15	32.60	29.31	31.83

Table 2
PSNR (dB) results of the proposed model with $a = 8,\ b = -1$ for various noise levels. At each noise level 'noisy' column represents the PSNR of the noisy image and 'result' the resultant image by our scheme.

Noise images	$\sigma_n = 5$		$\sigma_n = 10$		$\sigma_n = 15$		$\sigma_n = 20$	
	Noisy	Result	Noisy	Result	Noisy	Result	Noisy	Result
Lena	37.18	38.14	32.04	33.53	30.19	32.60	29.32	31.53
Cameraman	37.22	38.43	32.22	33.80	30.42	32.24	29.53	31.28
Barbara	37.17	38.09	32.02	33.51	30.15	31.94	29.29	31.35
House	37.20	37.98	32.04	33.41	30.13	31.42	29.25	31.25
Baboon	37.15	37.65	32.01	32.93	30.06	31.09	29.33	31.13
Shapes	39.15	40.84	34.04	34.41	32.12	33.22	31.26	32.11
Peppers	37.18	38.30	32.13	33.87	30.20	33.23	29.35	32.22
Montage	37.19	38.92	32.08	34.72	30.22	33.82	29.38	32.81
Man	37.10	38.19	31.98	33.57	30.17	32.71	29.29	31.53
Boats	37.20	38.32	32.08	33.56	30.15	32.28	29.31	31.17

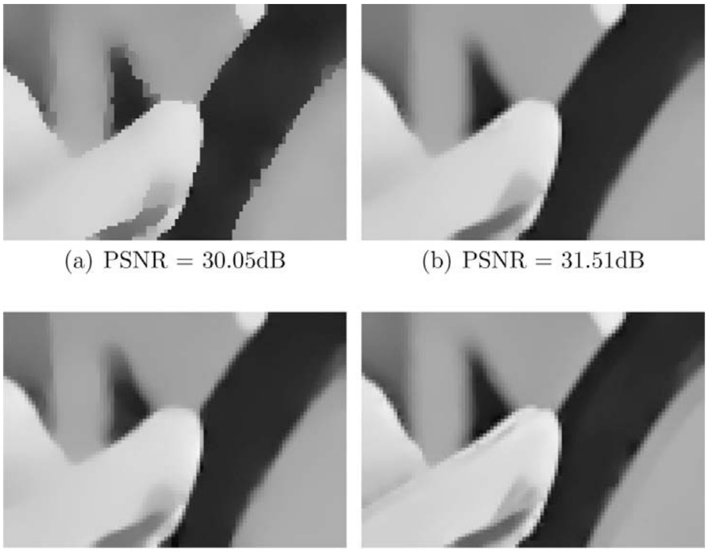

(a) PSNR = 30.05dB (b) PSNR = 31.51dB

(c) PSNR = 31.81dB (d) PSNR = 32.20dB

Fig. 9. Restoration result of *Lena* image (closeup from Fig. 4a) by different schemes: (a) Gauss-TV function [9]; (b) EFG filter [1]; (c) BFB filter [13] and (d) our scheme result.

image obtained by the proposed scheme when compared with the noisy image. The experiments conducted on a set of standard test images are tabulated. We stopped the time marching in (17) and (18) when the maximum PSNR value is achieved. This model is effective under extreme noise conditions (see the last column of Table 1 corresponding to noise level $\sigma_n = 20$).

Similar results are obtained for $b = -1$, as shown in Table 2. Increase in the PSNR value of magnitude 0.5 dB would be visible in the images. Other stopping time criteria can be used as in [15], for example using a priori information that the noise variance is σ_n^2. In this technique one sets $v_t = u_0 - u_t$, the residual part of the image estimated at time t. Then the diffusion is stopped at the time step t when variance of the residual part attains σ_n^2.

Finally, we compare our method to that of Gauss-TV filter [9], EFG filter [1], and BFB filter [13]. Fig. 9 shows a closeup of *Lena* image from Fig. 4 restored by these schemes with the result of our scheme with $b = 1$. Gauss-TV filter (Fig. 9a) removes noise but noise remain along edges due grey scale gradients. EFG and BFB filters avoid these artifacts (Fig. 9b and c) with EFG filter giving a smoother result than BFB filter. This also is inline with the observations from the comparative study [2] of these filters. On the other hand, the performance of our filter (Fig. 9d) is comparable to EFG and it removes noise and preserves a broad range of gradient scales.

6. Conclusions

We note that the existence and uniqueness result in Theorem 2 holds for the class of all strictly convex functions with Lipschitz continuous derivatives. We have proved the existence and uniqueness of our model using mild assumptions on the integrand of E. The simplicity of the result ensures the global convergence of our model. The price to pay for it is that the corresponding diffusion coefficient $g(.)$ is positive and must not decrease faster than that shown in (Fig. 1). In contrast, the classical Perona–Malik diffusion coefficients [6] decrease faster and the corresponding ϕ is non-convex. The choice of negative values of the parameter b gives impressive experimental results in image restoration. Theoretically the existence of a minimizer for the corresponding ϕ-function formulation remains open. We had chosen $b < 0$ in such a way that the diffusion function g remains positive hence the forward diffusion. Here our goal was to obtain a correct and simple theory of what can be a 'spatially adaptive convex variational model'. The proposed model restores the images without destroying the edges which is essential in low level vision. Exploring the above scheme more thoroughly for color images and sequences, and devising more robust numerical schemes constitute our future task.

Acknowledgements

The authors gratefully acknowledge the anonymous reviewers for their insightful comments which vastly improved the content and presentation of the paper. The authors are thankful to them, for pointing out relevant references and pointers to the literature, and to Prof. Melvin Scott for his time and efforts.

References

[1] K. Ito, K. Kunisch, Restoration of edge-flat-grey scale images, Inverse Probl. 16 (2000) 909–928.
[2] S.L. Keeling, Total variation based convex filters for medical imaging, Appl. Math. Comput. 139 (2003) 101–119.
[3] G. Aubert, P. Kornprobst, Mathematical Problems in Image Processing: Partial Differential Equation and Calculus of Variations, Applied Mathematical Sciences, second ed., vol. 147, Springer Verlag, New York, 2006.
[4] A.N. Tikhonov, V.Y. Aresenin, Solutions of Ill-Posed Problems, John Wiley, New York, 1977.
[5] G. Aubert, L. Vese, A variational method in image recovery, SIAM J. Numer. Anal. 34 (1997) 1948–1979.
[6] P. Perona, J. Malik, Scale-space and edge detection using anisotropic diffusion, IEEE Trans. Pattern Anal. Mach. Intell. 12 (1990) 629–639.
[7] D. Strong, T. Chan, Edge-preserving and scale-dependent properties of total variation regularization, Inverse Probl. 19 (2003) 165–187.
[8] L. Rudin, S. Osher, E. Fatemi, Nonlinear total variation based noise removal algorithms, Physica D 60 (1992) 259–268.
[9] A. Chambolle, P.L. Lions, Image recovery via total variation minimization and related problems, Numer. Math. 76 (1997) 167–188.
[10] A. Blake, A. Zisserman, Visual Reconctruction, MIT Press, Cambridge, MA, 1987.
[11] E. Zeidler, Nonlinear Functional Analysis and its Applications II, Springer Verlag, Berlin, 1990.
[12] S. Kichenassamy, The Perona–Malik paradox, SIAM J. Appl. Math. 57 (5) (1997) 1328–1342.
[13] S.L. Keeling, R. Stollberger, Nonlinear anisotropic diffusion for multiscale edge enhancement, Inverse Probl. 18 (2002) 175–190.
[14] S.L. Keeling, R. Bammer, F. Fazekas, R. Stollberger, Total variation denoising for improved diffusion tensor calculation, ISMRM 2000, Denver, CO, April 1–7, 2000.
[15] G. Gilboa, N. Sochen, Y.Y. Zeevi, Estimation of optimal PDE-based denoising in the SNR sense, IEEE Trans. Image Process. 15 (2006) 2269–2280.